Modeling, Simulation and Design of Piezoelectric Micro-Hydraulic Transducer Devices

O. Yaglioglu*, Y.H. Su**, D.C. Roberts*, J. Carretero* and N. W. Hagood*

*Active Material and Structures Laboratory, Massachusetts Institute of Technology, 77 Massachusetts Avenue, Rm. 37-315, Cambridge, MA 02139, onnik@mit.edu
**State University of New York, Stony Brook, NY

ABSTRACT

This paper reports on modeling, simulation and design considerations for piezoelectric Micro-Hydraulic Transducer (MHT) systems, focusing on power generation applications. Since these devices are complex fluid and structural systems, comprehensive simulation tools are needed for effective design. A system level simulation tool has been developed using Simulink^{TM}, by integrating models for different energy domains, namely fluids, structures, piezoelectrics and circuitry. The simulation allows for the monitoring of important parameters such as chamber pressure, flowrate, and various structural component deflections and stresses. Using the simulation, the operation of the system is analyzed and important design considerations are evaluated. Results indicate that system efficiency is highly dependent on compliances within the device structure and the type of piezoelectric material used.

Keywords: microhydraulic, power generation, piezoelectric

1 CONFIGURATION AND OPERATION

Piezoelectric Micro-Hydraulic Transducers are compact high power density transducers, which can function bi-directionally as actuators/micropumps and/or power generators. These devices are comprised of a main pumping chamber, two actively controlled valves, a low-pressure reservoir and a high-pressure reservoir (Figure 1) [1].

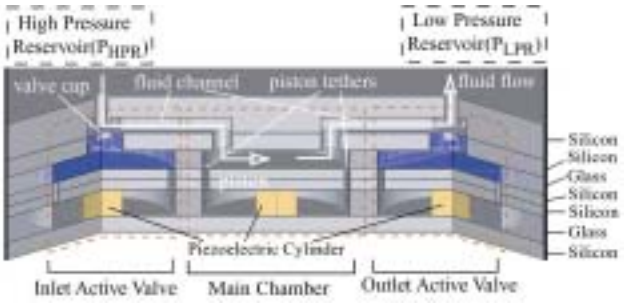

Figure 1: Device layout for power generator configuration. Top and bottom packaging pyrex layers not shown.

The active valves regulate fluid flow from the reservoirs into and out of the main chamber, which houses a piezoelectrically driven tethered piston. When operating as a pump, the electrical signal applied to the piezoelectric element results in pressure fluctuations inside the main chamber. When operating as a power generator, pressure fluctuations within the main chamber are converted to an electrical signal, which is rectified and stored in a battery. These devices are designed to generate 0.5-1W power at frequencies of ~15-20kHz, resulting in high power densities approaching 500-1000W/kg. This paper primarily focuses on modeling simulation and design considerations for MHT devices used as power generators.

A prototype MHT device consists of a 9-layer stack of pyrex and silicon micromachined layers (Figure 2). Sealing of the piston in the main chamber is provided by annular tethers which are created through Deep Reactive Ion Etching (DRIE) of a SOI wafer. The tether thickness (~10_m) is defined by the SOI device layer, and the buried oxide acts as an etch stop. All glass layers are patterned by conventional diamond core drilling. Piezoelectric cylinders are core drilled from piezoelectric substrate plates, onto which Ti-Pt-AuSn-Au multilayer film is sputter-deposited for eutectic bonding. The device assembly is accomplished through anodic bonding of the glass layers to the silicon layers at 300^{o}C, a process which also enables the AuSn eutectic alloy to melt. Upon cooling, the alloy solidifies, bonding the piezoelectric cylinders to the silicon layers. [2].

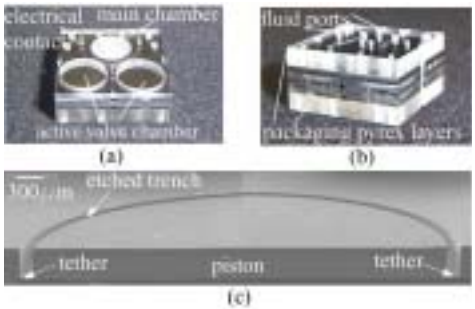

Figure 2: (a) 5-layer device for subcomponent testing (b) Complete 9-layer device (c) SEM of micromachined tethered piston structure.

2 MODELING

This section focuses on the development of a system level model to capture the behavior of the main chamber

portion of an MHT device under various operation conditions. The individual components considered for the main chamber are shown in Figure 3.

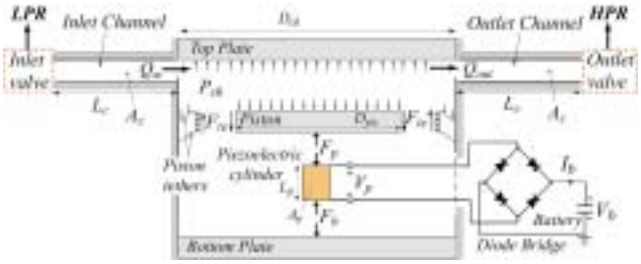

Figure 3: Modeling schematic of the main chamber and fluid channels. The active valves are not shown.

2.1 Piezoelectric Cylinder and Circuitry

Linear piezoelectric constitutive relationships are assumed. For a cross-sectional area A_p and length L_p, the net deflection of the piezoelectric element and the voltage across it can be expressed as:

$$x_p = \frac{L_p}{A_p}\left(s_{33}^D F_p + \frac{d_{33}}{\varepsilon_{33}^T} Q_p\right) \tag{2a}$$

$$V_p = \frac{L_p}{A_p}\left(\frac{d_{33}}{\varepsilon_{33}^T} F_p - \frac{1}{\varepsilon_{33}^T} Q_p\right) \tag{2b}$$

where Q_p is the charge, F_p is the force on the piezoelectric cylinder, s_{33}^D is the open circuit compliance, d_{33} is the piezoelectric constant and ε_{33}^T is the dielectric constant at constant stress for the case of compression parallel to polarization of the element. The governing equations for the diode bridge rectifier are derived using Kirchoffs laws and diode equations.

2.2 Chamber Continuity

The chamber converts hydraulic energy into mechanical energy via the piston, which then compresses the piezoelectric cylinder. Considering a control volume inside the chamber the continuity equation can be derived as:

$$\frac{dP_{ch}}{dt} = \frac{1}{C_{eff}}\left(Q_{in} - Q_{out} - \frac{dx_p}{dt} A_{pis}\right) \tag{3}$$

where P_{ch} is the chamber pressure, Q_{in} and Q_{out} are the flowrates into and out of the chamber respectively, x_p is the deflection of the piston, A_{pis} is the area of the piston and C_{eff} is the effective chamber compliance which is given by:

$$C_{eff} = \left(\frac{V_o}{\beta_f} + C_s\right) \tag{4}$$

where the first and second term correspond to the fluidic compliance (V_o is the initial volume of the chamber and β_f is the bulk modulus of the working fluid) and structural compliance, respectively. It is assumed that the volume displaced by the piston is much smaller than the initial volume of the chamber, V_o.

2.3 Structural Compliance

The structural compliance of the main chamber can be defined as:

$$C_s = \frac{\Delta V_s}{\Delta P_{ch}} \tag{5}$$

which represents the volume change of the chamber due to structural deformations in response to a change in chamber pressure. Individual structural compliances include the deformation of the top and bottom support structures, deformation of the piston and bending of the tethers. These deformations are calculated using linear plate theory [6]. Compliances of individual structural members act like parallel capacitors in an electric circuit analogy. Also, the stress distribution in the tether is calculated using linear plate theory. Finite-element models are then used to define appropriate stress concentration coefficients based on the fillet radius geometry [7]. In order to monitor important parameters in the simulation, such as chamber pressure, tether stress and volume changes due to individual members, the elastic equations of the respective components are simultaneously solved and the coefficients are fed to the Simulink™ simulation architecture (Figure 4). Additionally, within the simulation, look-up tables are incorporated which capture the non-linear large deflection behavior of the valve membrane structures [5]. A numerical code [4] is used to generate these look-up tables.

2.4 Valves and Channels

During system operation, the flow in the channels is inertia dominated due to the high Reynolds numbers. The valves are modeled using orifice flow relations. The form of the governing equations for the valves and the channels are as follows:

$$P_{HPR} - P_{ch} = R_i(Q_{in}, vo_{in})Q_{in}^2 + \left(\frac{\rho L_c}{A_c}\right)\frac{dQ_{in}}{dt} \tag{6a}$$

$$P_{ch} - P_{LPR} = R_o(Q_{out}, vo_{out})Q_{out}^2 + \left(\frac{\rho L_c}{A_c}\right)\frac{dQ_{out}}{dt} \tag{6b}$$

where P_{HPR} and P_{LPR} are the pressures of the high and low pressure reservoirs, L_c and A_c are the length and the cross sectional area of the fluid channels, and R_i and R_o are the flow resistances in the inlet and outlet valve, respectively, which are calculated based on the flowrate, the valve opening (vo_{in} ,vo_{out}) and the valve geometry using look-up

tables where experimental discharge coefficients are incorporated into the simulation[3].

3 SIMULATION AND ANALYSIS

The equations and look up tables described in the previous section are incorporated into the Matlab™/Simulink™ simulation software, as shown in Figure 4. The basic input/output relationships between the modules correspond to subcomponents of the device. Additional monitored parameters such as stresses and deflections are included in the simulation, although not shown in the figure.

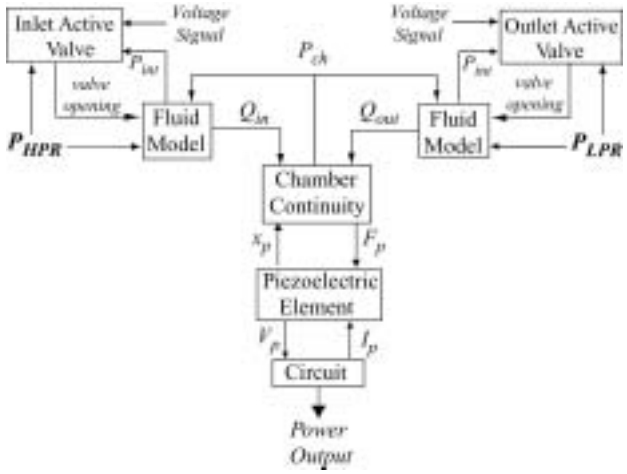

Figure 4: Modular Simulink™ simulation architecture for power generation configuration.

The device has been simulated for a sample geometry and operating conditions, where D_{pis}= 4.5mm, P_{HPR}=2MPa, P_{LPR}=0MPa, f=10kHz and V_b=90V. The battery voltage is equal to one fourth of the open circuit voltage of the piezoelectric element for maximum power output. The valve size is determined such that the chamber pressure fluctuates between P_{HPR} and P_{LPR}. The time histories, which represent a typical duty cycle of the power generator, are shown in Figure 5. The corresponding force vs. deflection plot (i.e. the work cycle of the piezoelectric element) is shown in Figure 6).

The average flow rate can be found by integrating equation 3 to obtain:

$$Q_{ave} = A_{pis}\Delta x_p f + C_{eff}\Delta P_{ch} f \tag{7}$$

where $\_x_p$ is the net piston deflection, $\_P_{ch}$ is the maximum pressure difference in the chamber and f is the operation frequency.

The electrical energy stored per cycle is equal to the area enclosed by the work cycle shown in Figure 6. The generated power can be obtained:

$$W = \frac{1}{4}(s_{33}^E - s_{33}^D)\sigma_d^2 A_p L_p f \tag{8}$$

where $\__d$ is the maximum stress on the piezoelectric element.

For negligible bottom plate deflection, the net piston deflection in a cycle is equal to the net compression of the piezoelectric cylinder, which can be expressed as:

$$\Delta x_p = \frac{1}{2}\sigma_d L_p (s_{33}^E + s_{33}^D) \tag{9}$$

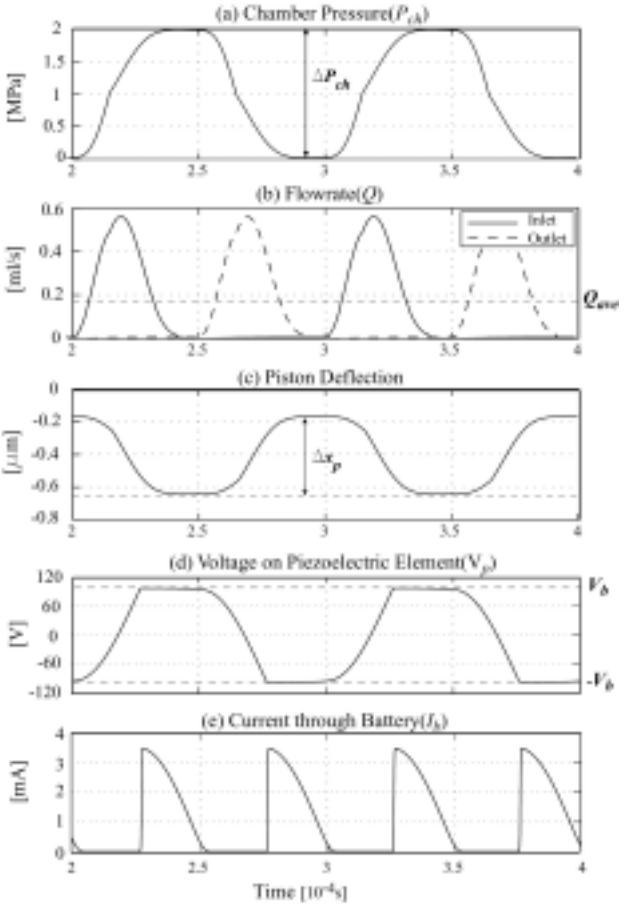

Figure 5: Typical duty cycle of the power generator. Generated power is equal to $V_b I_b$.

Using equations 7, 8 and 9 and assuming that the maximum pressure in the chamber is P_{HPR}, and the minimum pressure is zero, the average flow rate required for a given power requirement, W, can be calculated as:

$$Q_{ave} = \frac{2(s_{33}^E + s_{33}^D)W}{(s_{33}^E - s_{33}^D)P_{HPR}} + C_{eff} P_{HPR} f \tag{10}$$

The first term in equation 10 corresponds to the flowrate required to move the piston and the second term corresponds to the additional flowrate required due to the chamber compliance.

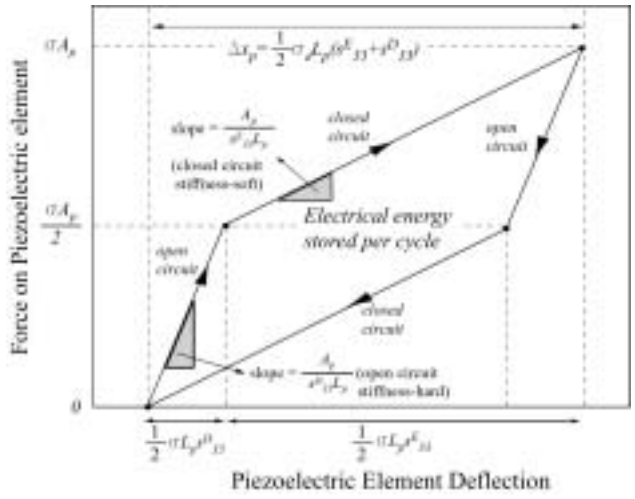

Figure 6: The work cycle of the piezoelectric element.

4 DESIGN CONSIDERATIONS

Tether Optimization: The tether structure has to be flexible enough to allow piston movement, yet stiff enough such that the additional compliance introduced by the tether is minimal. Also, the maximum stress shouldn't exceed 1GPa [8]. Tether thickness and width optimization studies have been performed, but are not covered in this paper.

Fluidic Oscillations: The fluid channels and the main chamber constitute a resonating system similar to a Helmholtz resonator. The L_c/A_c ratio of the fluid channels should be chosen such that it will satisfy the resonance conditions at the design frequency. The simulation tool is used for these studies.

Piezoelectric Material and Efficiency: The efficiency of the chamber, neglecting power consumption in the valves, can be calculated by dividing the electrical power output by the hydraulic power input. The maximum possible efficiency, which corresponds to the case where the effective chamber compliance C_{eff} is zero, can be obtained from equation 10:

$$\eta_{\max} = \frac{W}{Q_{\min} P_{HPR}} = \frac{k_{33}^2}{4 - 2k_{33}^2} \qquad (11)$$

where Q_{min} is the minimum required flowrate and k_{33} is the coupling coefficient of the piezoelectric element. Piezoelectric materials differ in their depolarization stress, $\_d$, which determines the power density of the material, and coupling coefficient, k_{33} which determines the electromechanical energy conversion efficiency. Figure 7 shows a comparison of different piezoelectric materials in terms of system efficiency for the geometry discussed in the previous section and for a $0.5W$ power requirement. It can be seen that the single crystal piezoelectric material PZN-PT is the most efficient material because of its very high coupling coefficient. However, due to its low depolarization stress, it requires higher operational frequencies. The designed bandwidth of the active valves is ~20kHz and the operation frequency of the device should be below this value. Tradeoffs such as this need to be carefully considered in the design procedure.

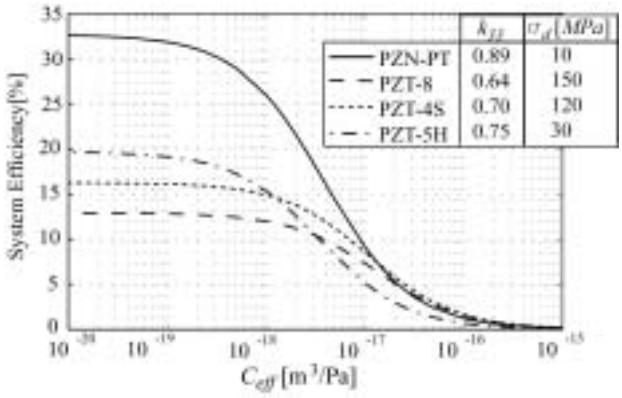

Figure 7: Comparison of different piezoelectric materials.

Using the simulation and the analysis discussed, design procedures have been carried on for building prototype MHT devices. Major design limitations are the depolarization stress of the piezoelectric material and maximum allowable stress in the tethers. Typical efficiencies are ~15%. The main chamber design is complimented by the design of the active valves, detailed in [5].

5 CONCLUSIONS

A system level simulation tool has been developed which allows dynamic simulation of linear and nonlinear structural members, micro-fluid flow, piezoelectrics, circuitry and monitoring of important system parameters in different energy domains. The system is analyzed for power generator configuration and important design considerations are investigated. It is found that system efficiency highly depends on structural compliances and the type of piezoelectric material used.

REFERENCES

[1] N.W. Hagood *et al,* Proceedings of SPIE, Vol. 3985 (2000), pp. 680-688.

[2] D.C. Roberts *et al,* Transducers 2001, Munich, Germany, June 2001.

[3] J. Carretero *et al,* Proceedings of the ASME Microfluidics Symposium. Orlando, FL. Nov. 2000.

[4] Y.H. Su, *et al*, Journal of Micromechanics and Microengineering. 11 (2001), pp.645-653.

[5] D.C. Roberts *et al*, Proceedings of SPIE, Vol. 4327 (2001), pp.366-380.

[6] S. Timoshenko, Theory of Plates and Shells, McGraw-Hill, New York, 1940.

[7] K. Turner, S.M Thesis, MIT, 2001.